# Body Forces Drive the Apparent Line Tension of Sessile Droplets

Beng Hau Tan,[1] Hongjie An,[2,*] and Claus-Dieter Ohl[3]
[1]KB Corporation, The Plaza, 7500A Beach Road, 199591, Singapore
[2]Queensland Micro and Nanotechnology Centre, Griffith University, 170 Kessels Road, Nathan, Queensland 4111, Australia
[3]Institute of Physics, Otto von Guericke University Magdeburg, Universitätsplatz 2, 39016 Magdeburg, Germany

(Received 13 May 2022; accepted 5 December 2022; published 8 February 2023)

The line tension of a three-phase contact line is implicated in a wide variety of interfacial phenomena, but there is ongoing controversy, with existing measurements spanning six orders of magnitude in both signs. Here, we show that computationally obtained magnitudes, sign changes, and nontrivial variations of apparent line tension can be faithfully reproduced in a parsimonious model that incorporates only liquid-substrate interactions. Our results suggest that the origin for the remarkable variation lies in the failure of a widely used estimation method to eliminate body forces, leading measured line tensions to behave like an extensive quantity.

DOI: 10.1103/PhysRevLett.130.064003

Wetting and interfacial phenomena are characterized by quantities emergent at the nexus of bulk phases. For example, the surface tension is the excess free energy per unit area of the surface at which two bulk phases meet. Similarly, three phases meet at a line for which the excess free energy per unit length defines the line tension [1]. A precise determination of these quantities is crucial for the understanding and systematic control of natural and industrial phenomena mediated by wetting effects, including heterogeneous nucleation [2], cavity drying [3,4], or the fabrication of functional materials [5–8].

The surface tension $\gamma$ is well understood, with computational and experimental studies [9–11] on a wide variety of phase pairs, length scales, and techniques estimating $\gamma \sim 10^{-1}$ N/m. This estimate comports with the simple dimensional estimate $\gamma \sim k_B T/a_0^2$, assuming a length scale of $a_0 \sim 1$ Å and a thermal energy $k_B T$. Surprisingly, there is no such consensus about the line tension $\tau$. Decades of experiments [12–25] and simulations [26–30] yield measurements that span six orders of magnitude, $10^{-12} < \tau < 10^{-6}$ N, in sharp contrast with the expected $\tau \sim k_B T/a_0 \sim 10^{-11}$ N. Furthermore, measured $\tau$ varies nonmonotonously and changes sign with changing system size and wettability [31].

The line tension is predominantly estimated by the contact angle measurements of liquid droplets on solid surfaces [31,32]. Although Young's equation, $\cos\theta_0 = (\gamma_{SG} - \gamma_{LS})/\gamma_{LG} = \Delta\gamma/\gamma_{LG}$ ($S$, $L$, and $G$ denote the liquid, solid, and gas phases) predicts that droplet contact angles $\theta$ are size independent, a size dependence is ubiquitously observed in practice. This effect is modeled by incorporating a phenomenological line tension $\tau$ into a corrected Young equation [33,34]

$$\cos\theta = \cos\theta_0 - \frac{\tau}{a\gamma_{LG}}, \tag{1}$$

where $a$ is the footprint radius; see Fig. 1. As Young's equation is derivable from a force balance, $\tau$ can be interpreted as an effective force, driving droplets to adopt smaller or larger contact angles [12].

Whereas the $\tau$ measured by Eq. (1) was originally envisaged to be the sought-after *intrinsic* line tension $\tau_i$, the contemporary view supposes that all measured $\tau$ should instead be considered as an apparent line tension $\tau_a$ arising from an inextricable combination of the intrinsic value and other secondary effects, including the Tolman effect [35], contact angle hysteresis from surface roughness [32], and measurement errors [36]. It is, however, still unclear which particular factors drive the apparent line tension. The influential monograph of de Gennes *et al.* [36] argued that large micronewton line tensions observed optically are an artifact of experimental error. Although the idea that measurements are affected by numerous sources of error is uncontroversial, a collection [37] of 20 years of

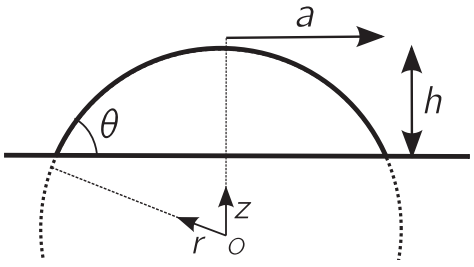


FIG. 1. Schematic of a sessile droplet in axisymmetric coordinates with footprint radius $a$, height $h$, contact angle $\theta$, and radius of curvature $r$ on a solid substrate.

 

experimental data shows that $\tau_a$ scales with droplet size $a$ over five orders of magnitude: an observation difficult to attribute entirely to random experimental error.

In this Letter, we explore the possibility that the size variation of apparent line tension is driven by a universal factor present in all wetting systems. Through a minimal model, we show that body forces alone are capable of reproducing magnitudes and nontrivial variations in the apparent line tension.

We begin by sketching out the derivations of both the Young equation and the line tension relation [Eq. (1)] in a droplet with a footprint radius $a$ and height $h$; see Fig. 1. Our calculations operate in an axisymmetric coordinate system for which the origin $O$ is the droplet's centroid. Expressed as a function of $\theta$ and the radius of curvature of $r = a/\sin\theta$, the free energy $E$ of a sessile droplet on a plane surface is

$$E(r,\theta) = 2\pi\gamma_{LG}r^2(1-\cos\theta) + (\gamma_{SG}-\gamma_{LS})\pi r^2\sin^2\theta. \quad (2)$$

Young's equation emerges from the minimization of Eq. (2). Because $r$ and $\theta$ are mutually dependent, derivatives of $E$ with respect to each of these variables must consider the exact differential

$$dE = \left(\frac{\partial E}{\partial\theta} + \frac{\partial E}{\partial r}\frac{dr}{d\theta}\right)d\theta = 0.$$

The unknown $dr/d\theta$ can be obtained by exploiting incompressibility, i.e.,

$$dV = \frac{\partial V}{\partial\theta}d\theta + \frac{\partial V}{\partial r}dr = 0,$$

and taking partial derivatives of the volume of a spherical cap

$$V(r,\theta) = \frac{\pi r^3}{3}(2+\cos\theta)(1-\cos\theta)^2.$$

A surprisingly tedious effort (see the Supplemental Material [38]) simplifies to Young's equation,

$$(\gamma_{SG}-\gamma_{LS}) + \gamma_{LG}\cos\theta_0 = 0. \quad (3)$$

To incorporate an intrinsic line tension $\tau_i$, one adds to Eq. (2) the phenomenological term [33] $\Delta E_\tau = 2\pi r\sin\theta\tau_i$, where $2\pi r\sin\theta$ is the perimeter of the droplet's three-phase line. Minimizing $E + \Delta E_\tau$ with respect to $\theta$ yields Eq. (1) (see the Supplemental Material [38]).

The aforementioned argument omits body forces: an assumption that clearly breaks down at some length scales. A millimetric droplet ($r = 10^{-3}$ m) has gravitational potential energy of $\Delta E_g(r) \sim \rho g r^4 \sim 10^{-8}$ J, which is comparable to $E \sim 10^{-8}$ J. Evaluating $\Delta E_g = \int \rho g z dV$ as a volume of revolution leads to

$$\Delta E_g = \rho\pi g\int_{r-h}^{r}(z-(r-h))(r^2-z^2)dz = \frac{\rho g\pi r^4}{12}(3+\cos\theta)(1-\cos\theta)^3.$$

Minimizing $E + \Delta E_g$ (with regard to $\theta$) produces [39,40]

$$(\gamma_{SG}-\gamma_{LS}) + \gamma_{LG}\cos\theta - \frac{\rho g r^2}{6}(1-\cos\theta)^2 = 0, \quad (4)$$

for which the root is the expected contact angle $\theta$ in a gravitational field. Notably, Eq. (4) implies $\tau_a \sim +10^{-6}$ N for a millimetric droplet [Fig. S1], which is in surprisingly good agreement with experimental measurements [13,22,32].

We now extend this analysis to explore a nanoscopic analogy to the gravitational case: specifically, the widely studied system of water on a graphenelike substrate. Assume that the interaction between a single liquid molecule and the adjacent surface is mediated by a uniaxial potential $\phi(z')$. Here, we designate the separation distance to the adjacent substrate as $z'$ to make a distinction from the $z$ coordinate in Fig. 1. An incompressible control volume $dV$ of the liquid contains $\rho_n dV$ molecules, where the number density $\rho_n$ is a constant $\rho_n^0 = 30\,\text{Å}^{-3}$ in bulk liquid but adjacent to the substrate,

$$\rho_n(z') = \rho_n^0\exp(-\phi(z')/\eta k_B T). \quad (5)$$

Here, $k_B$ is the Boltzmann constant, $T = 300$ K is the temperature, and $\eta$ is a dimensionless scaling factor for which the utility will be explained later. Summing up the scaled liquid-substrate interaction for all liquid molecules in a spherical cap droplet of height $h \equiv r(1-\cos\theta)$ through an axisymmetric volume of revolution integral yields

$$\Delta E_\phi = \int_{r-h+\delta}^{r}\rho_n(z-r+h)\frac{\phi(z-r+h)}{\eta}\pi(r^2-z^2)dz. \quad (6)$$

In the continuum limit, $\delta$ should ordinarily be zero; but, in molecular dynamics (MD) simulations, short-ranged repulsion produces a gap $\delta$ between the substrate and the first liquid molecule; following Kim *et al.* [41], we use $\delta = 3$ Å. Our calculations assume the potential $\phi$ (with dimension of energy) between water and the substrate is governed by the 10-4 form [42]

$$\phi(z') = 4\pi\varepsilon_{\text{CO}}d\left(\frac{\sigma_{\text{CO}}^{12}}{5z'^{10}} - \frac{\sigma_{\text{CO}}^{6}}{2z'^{4}}\right), \quad (7)$$

using Lennard-Jones 12-6 parameters for a system of SPC/E water on a graphene lattice [43]. The 12-6 Lennard-Jones interactions between individual liquid-substrate atoms, when integrated over a planar surface, produce a

9-3 liquid-wall potential (see Supplemental Material [38]) that would be a logical choice for $\phi$. However, the minimum of the 9-3 potential is known to be too close to the substrate. Steele's 10-4 potential was developed as a replacement that avoids this issue [44,45]. The distance parameter between carbon (C) and oxygen (O) is set as $\sigma_{CO} = 3.19$ Å, and $d = 38.1$ nm$^{-2}$ is the surface density of substrate atoms on a graphene lattice. Finally, we use the empirical equation [Eq. (4)] of Werder *et al.* [43] to establish a first-order estimate for the relationship between the Lennard-Jones energy parameter $\varepsilon_{CO}$ and the Young contact angle $\theta_0$.

The potential [Eq. (7)] overestimates the true interaction strength because its substitution in Eq. (5) implies that the maximum density adjacent to the surface will reach an unrealistically large maximum of about 8 g/cm$^3$ [41]. This value is unphysical because water will crystallize at such high densities and, more importantly, because it is far larger than the 2–3 g/cm$^3$ found in MD simulations [12,41]. A common way to ease this discrepancy [41,46,47] is to scale the magnitude of $\phi$ by a system-specific dimensionless factor $\eta$ such that the density peak predicted by Eq. (5) matches that observed computationally; for the SPC/E water-graphene system, $\eta \approx 7.16$ [47], which we use in our calculations.

We implement our model numerically by (1) computing Eq. (6) with Gauss quadrature; (2) computing partial derivatives in $r$ and $\theta$ via finite differences; and finally, (3) calculating $\theta(a)$ by solving for the roots of the ensuing equation

$$\gamma_{SG} - \gamma_{LS} + \gamma_{LG}\cos\theta - \frac{2+\cos\theta}{2\pi r^2 \sin\theta}\frac{d}{d\theta}[\Delta E_\phi(r,\theta)] = 0. \quad (8)$$

Details of the numerical implementation, derivations of Eq. (8) and each contribution explored in this Letter, and validation efforts are chronicled in the Supplemental Material [38].

We present the predicted contact angles of water droplets on a graphenelike substrate for which the Young angles have been varied across $40 < \theta_0 < 140°$; see Fig. 2. By specifying this range of $\theta_0$, we do not mean to imply that water adopts a wide variation of contact angle on graphene; rather, we are mimicking the widespread practice of modulating surface wettability *in silico* through $\varepsilon_{CO}$. Each curve terminates when any of the droplet's spatial dimensions $(a, h)$ fall below 0.5 nm. As seen in Fig. 2(a), each $(\theta, a)$ curve follows a similar dependence from the large to small droplet limit; the contact angle becomes smaller, reaches a minimum, and increases again, concomitant with the well-shaped spatial variation of the potential $\phi(z)$. Although each curve observes a qualitatively similar variation, the position of the minimum is offset with an increasing contact angle such that the minimum disappears for $\theta_0 \gtrsim 100°$. Although a quantitative comparison to previous MD studies is complicated by the selection of different water-substrate models, simulation run times, and sampling intervals in each study, we note that the detailed contact angle variations seen in Fig. 2 are qualitatively reproduced in both hydrophilic and hydrophobic systems (see Fig. 4 of [27], Fig. 3(a) of [12], and Fig. 7 of [29]).

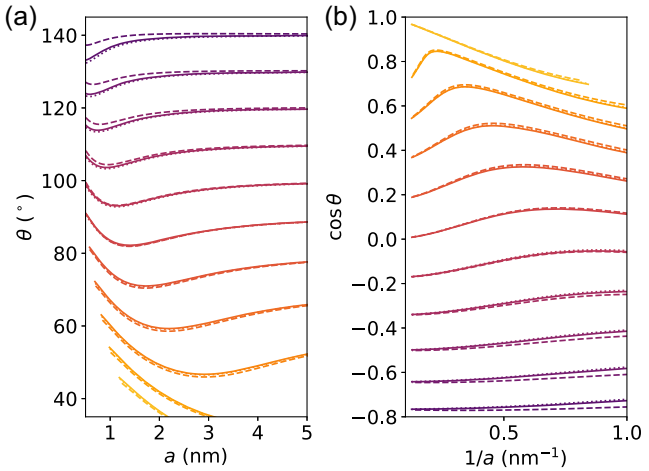


FIG. 2. The intermolecular liquid-substrate attraction manifests as an apparent line tension for nanoscale droplets in the (a) $\theta(a)$ representation, and (b) $\cos\theta(1/a)$ representation. Solid lines correspond to the baseline case incorporating only body forces [Eq. (8)]. The Tolman effect for $\delta_T = 0.5$ nm (dashed lines) or an intrinsic line tension $\tau_i = -5$ pN (dotted lines, but obscured by the baseline case) produces only a marginal change. All curves terminate when any spatial dimension falls below 0.5 nm.

Unlike in experiments, MD simulations allow for line tensions to be estimated over a continuous range of wettabilities by tuning $\varepsilon_{CO}$. Parameter studies usually find that $\tau_a < 0$ for small $\theta_0$ and $\tau_a > 0$ for large $\theta$, with a sign crossover at intermediate wettability. Combined, these features lead to a characteristic asymmetric U-shaped curve that is seen in a variety of substrates including atomically flat and rigid substrates of graphene [27] and fcc geometries [12], as well as mobile, nonatomically flat polar surfaces [26]. To mimic computational estimates of $\tau_a$ from MD simulations, we perform a linear regression of $\cos\theta$ and $1/a$ for changing wettability $\theta_0$ as per Eq. (1), limiting the range of droplet sizes used in the regression to the MD scale of $2 < a < 8$ nm. Our model captures the characteristic $\tau \sim 10$ pN magnitude and reproduces the U-shaped $\tau_a(\theta)$ curve; see Fig. 3.

Our model has so far neglected the intrinsic line tension $\tau_i$, although it is anticipated to contribute to the apparent line tension. Widely known issues with inferring line tension from contact angle measurements have inspired new computational techniques of estimating $\tau_i$ that avoid scale dependence. Consequently, three independent computational estimates [48–50] suggest $\tau_i$ is in the region of $-5$ pN. To understand how this scenario influences our predictions, we incorporate $\tau_i = -5$ pN into our model [Eq. (8)]. The size-angle distributions $\theta(a)$ and inferred

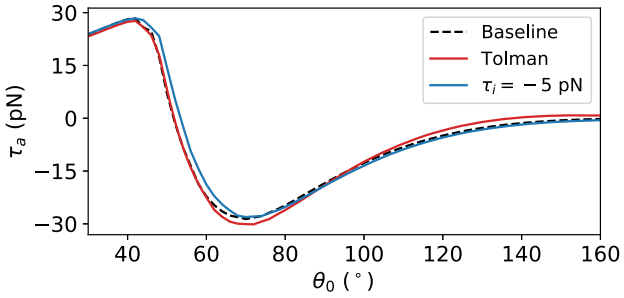


FIG. 3. Predicted apparent line tension $\tau_a(\theta)$ as a function of wettability. The apparent line tension is calculated from a linear regression of droplet sizes, $2 < a < 8$ nm, to Eq. (1). This procedure produces an asymmetric U-shaped curve featuring a positive $\tau$ hydrophilic limit, negative $\tau$ in the hydrophobic limit, and a sign crossover at intermediate $\theta_0$. Curves qualitatively similar in both shape and magnitude (i.e., $\tau \sim 10$ pN) have been reported in MD simulations of water on various substrates [12,26,27]. The Tolman effect ($\delta_T = 0.5$ Å, red) and intrinsic line tension ($\tau_i = -5$ pN, blue line) produce only a small change from the baseline case ($\tau_i = 0$, black dashed line).

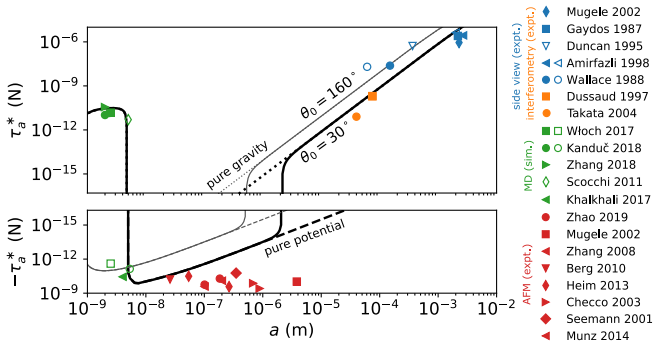


FIG. 4. Body forces explain the remarkable variation of $\tau_a^*$ in experiments and simulations. Model predictions are shown for hydrophobic (thin line, $\theta_0 = 160°$) and hydrophilic (thick line, $\theta_0 = 30°$) wettabilities; only the effects of gravity and intermolecular forces are included ($\tau_i = 0$). These predictions compare well against previous experiments [side view optical imaging, blue; interferometry, orange; atomic force microscopy (AFM), red] and simulations (MD, green). Filled points represent droplets on hydrophilic surfaces, and hollow ones hydrophobic surfaces. The asymptotic behaviors of the potential and gravitational components alone are shown as dashed and dotted lines, respectively.

apparent line tensions for this case are shown in Figs. 2 (dotted lines) and 3 (blue line), respectively; only a numerically small change from the baseline case of $\tau_i = 0$ (black dashed line) is observed.

Another widely invoked influence on the apparent line tension is the Tolman effect: the dependence of surface tension on the curvature of the liquid-gas interface

$$\gamma_{\mathrm{LG}}(r) = \frac{\gamma_{\mathrm{LG}}}{1 + 2\delta_T/r}, \tag{9}$$

where $\delta_T$ is the Tolman length. Contemporary computational and experimental estimates [51–54] suggest $0.01 \lesssim \delta_T \lesssim 0.5$ Å. We modify our model [Eq. (8)] with Eq. (9) for $\delta_T = 0.5$ Å, producing contact angle $\theta(a)$ curves in dashed lines in Fig. 2 and predicted apparent line tension (red line) in Fig. 3. Again, the Tolman effect has only a small influence on the model predictions, albeit manifesting more strongly in the small droplet and hydrophobic limits. (Between two droplets of the same volume, the one with a larger contact angle has a smaller $r$.)

Our results therefore suggest that, at the nanoscale, the apparent line tension is predominantly driven by body forces, with the Tolman effect and the intrinsic line tension making only small contributions. These contributions are small even at the nanoscale, where they ought to be at their strongest, prompting the follow-up question: Do body forces drive the apparent line tension across all length scales?

To answer this question, we solve for the line tension variation $\tau_a^*(a)$ from the nanoscale to the macroscale, incorporating in Eq. (8) only a gravitational component and the short-ranged (∼1 nm) intermolecular component [Eq. (6)]; see Fig. 4. Note that our calculation of $\tau_a^*$ differs from that computed in Fig. 3; whereas the latter uses a regression over a specified range of droplet sizes, our calculation of $\tau_a^*(a)$ is pointwise, i.e., calculated from the numerical derivative of $\cos\theta$ as a function of $1/a$.

We plot in Fig. 4 two characteristic curves bookending the hydrophilic and hydrophobic limits, respectively, and compare these curves against apparent line tension estimates from both simulations ([26–30], points in green) and experiments (AFM [12–19], red; optical interferometry [21,25], orange; side view optical imaging [13,20,22–24], blue). Filled points correspond to droplets on hydrophilic surfaces, whereas hollow ones correspond to hydrophobic surfaces. For comparison, we also plot the behavior from the individual intermolecular and gravitational components in dashed and dotted lines, respectively. We limit our comparison to studies in which surfaces are smooth (i.e., ignoring nanostructured surfaces), which infer the apparent line tension only by Eq. (1), and which are free of significant contact angle hysteresis (deferring to the judgment of Amirfazli and Neumann in their authoritative review [32]).

Despite including only two body force contributions for the nanoscale and the macroscale, our model successfully reproduces the full, approximately six-order variation of $\tau_a$ central to the discrepancy between theory and observation, as shown in Fig. 4. As discussed earlier, we find good agreement between the model and simulations, with the one apparent exception being a positive line tension found for hydrophobic systems by Scocchi *et al.* [29]. This discrepancy arises because their estimate of $\tau_a$ omits small droplets on one side of an unexplained contact angle saturation (Fig. 7 of Ref. [29]), creating a V-shaped kink in the $\theta(a)$ representation. Our model reproduces the contact angle saturation in $\tau_a$ reported in Ref. [29], as seen in the upper left corner of Fig. 2(a). In the macroscopic regime, our model correctly captures

ubiquitous observations of large micronewton line tensions in the $10^{-5}$ to $10^{-4}$ range.

Our model underestimates the magnitude of line tension in the microscale regime of $10^{-7} < a < 10^{-6}$ m, but disagreement is within our expectations for two reasons. First, experiments in the microscale regime rely on tapping mode AFM to image droplets that, unlike the other techniques in our dataset, is inherently invasive. Successful imaging entails the probe exerting a finite interaction force that slightly deforms the droplet, generating a negative but spurious contribution to $\tau_a$. To complicate matters, experiments in the $a = 50$–$300$ nm regime [55] corroborate theoretical predictions [56,57] that the interfacial stiffness of droplets increases substantially with decreasing size. Under similar imaging conditions (set point in tapping mode), larger droplets experience a greater relative deformation, making a negative contribution to $\tau_a$ that lowers the curves in Fig. 4. Observed measurements are consistent with this argument, evidenced by the relatively good model agreement for small (∼10 nm) AFM-imaged droplets. An equally plausible but more straightforwardly articulated reason for our model's underestimate of $\tau_a$ in this regime is its omission of attractive body forces at the nanometer to micrometer range, for which the inclusion would lower the theoretical curves in Fig. 4, and thus improve agreement with the experimental data. We have not modeled this effect because there are numerous—possibly coexisting—possible long-ranged liquid-substrate interactions at the 1 nm [58,59], 10 nm [60–62], and 100 nm ranges [63,64].

In summary, we present a minimal model that demonstrates how the apparent line tension is primarily driven by body forces. Our results imply that the remarkable six-order discrepancy between observed and theoretical accounts of the line tension arises from the failure by measurement techniques to eliminate body forces, leading measured line tensions to behave like an extensive quantity (Fig. 4), despite being defined from the outset to be an intensive one. Recent computational estimates [49,50] that intentionally avoid scale dependence lend support to this picture because they yield some of the smallest known (approximately piconewton) measurements of the line tension. We envisage that our findings, allied with new measurement techniques uncontaminated by extensive contributions, will pave the way for much sought-after clarity about the line tension.

B. H. T. acknowledges productive discussions with Xianyue Chen. H. A. is supported by an ARC Future Fellowship.

*hongjie.an@griffith.edu.au

[1] J. W. Gibbs, *On the Equilibrium of Heterogeneous Substances* (New Haven, 1874), http://archive.org/details/Onequilibriumhe00GibbA.

[2] R. Bey, B. Coasne, and C. Picard, Carbon dioxide as a line active agent: Its impact on line tension and nucleation rate, Proc. Natl. Acad. Sci. U.S.A. **118** (2021).

[3] S. Sharma and P. G. Debenedetti, Evaporation rate of water in hydrophobic confinement, Proc. Natl. Acad. Sci. U.S.A. **109**, 4365 (2012).

[4] J. Zhang, F. Leroy, and F. Müller-Plathe, Influence of Contact-Line Curvature on the Evaporation of Nanodroplets from Solid Substrates, Phys. Rev. Lett. **113**, 046101 (2014).

[5] A. Nikoubashman, V. E. Lee, C. Sosa, R. K. Prud'homme, R. D. Priestley, and A. Z. Panagiotopoulos, Directed assembly of soft colloids through rapid solvent exchange, ACS Nano **10**, 1425 (2016).

[6] J. Aizenberg and G. Hendler, Designing efficient microlens arrays: Lessons from nature, J. Mater. Chem. **14**, 2066 (2004).

[7] L. Bao, B.-E. Pinchasik, L. Lei, Q. Xu, H. Hao, X. Wang, and X. Zhang, Control of femtoliter liquid on a microlens: A way to flexible dual-microlens arrays, ACS Appl. Mater. Interfaces **11**, 27386 (2019).

[8] J. Yu, Y. Yang, A. Liu, L. Chin, and X. Zhang, Microfluidic droplet grating for reconfigurable optical diffraction, Opt. Lett. **35**, 1890 (2010).

[9] T. W. Richards and E. K. Carver, A critical study of the capillary rise method of determining surface tension, with data for water, benzene, toluene, chloroform, carbon tetrachloride, ether and dimethyl aniline [second paper.], J. Am. Chem. Soc. **43**, 827 (1921).

[10] V. V. Zakharov, E. N. Brodskaya, and A. Laaksonen, Surface tension of water droplets: A molecular dynamics study of model and size dependencies, J. Chem. Phys. **107**, 10675 (1997).

[11] R. W. Style, R. Boltyanskiy, Y. Che, J. S. Wettlaufer, L. A. Wilen, and E. R. Dufresne, Universal Deformation of Soft Substrates Near a Contact Line and the Direct Measurement of Solid Surface Stresses, Phys. Rev. Lett. **110**, 066103 (2013).

[12] B. Zhao, S. Luo, E. Bonaccurso, G. K. Auernhammer, X. Deng, Z. Li, and L. Chen, Resolving the Apparent Line Tension of Sessile Droplets and Understanding Its Sign Change at a Critical Wetting Angle, Phys. Rev. Lett. **123**, 094501 (2019).

[13] F. Mugele, T. Becker, R. Nikopoulos, M. Kohonen, and S. Herminghaus, Capillarity at the nanoscale: An AFM view, J. Adhes. Sci. Technol. **16**, 951 (2002).

[14] X. H. Zhang and W. Ducker, Interfacial oil droplets, Langmuir **24**, 110 (2008).

[15] J. K. Berg, C. M. Weber, and H. Riegler, Impact of Negative Line Tension on the Shape of Nanometer-Size Sessile Droplets, Phys. Rev. Lett. **105**, 076103 (2010).

[16] L.-O. Heim and E. Bonaccurso, Measurement of line tension on droplets in the submicrometer range, Langmuir **29**, 14147 (2013).

[17] A. Checco, P. Guenoun, and J. Daillant, Nonlinear Dependence of the Contact Angle of Nanodroplets on Contact Line Curvature, Phys. Rev. Lett. **91**, 186101 (2003).

[18] R. Seemann, K. Jacobs, and R. Blossey, Polystyrene nanodroplets, J. Phys. Condens. Matter **13**, 4915 (2001).

[19] M. Munz and T. Mills, Size dependence of shape and stiffness of single sessile oil nanodroplets as measured by atomic force microscopy, Langmuir **30**, 4243 (2014).

[20] J. A. Wallace and S. Schürch, Line tension of a sessile drop on a fluid-fluid interface modified by a phospholipid monolayer, J. Colloid Interface Sci. **124**, 452 (1988).
[21] A. Dussaud and M. Vignes-Adler, Line tension effect on alkane droplets near the wetting transition, Mat Res Soc. Symp. Proc. **464**, 287 (1996).
[22] A. Amirfazli, D. Kwok, J. Gaydos, and A. Neumann, Line tension measurements through drop size dependence of contact angle, J. Colloid Interface Sci. **205**, 1 (1998).
[23] J. Gaydos and A. Neumann, The dependence of contact angles on drop size and line tension, J. Colloid Interface Sci. **120**, 76 (1987).
[24] D. Duncan, D. Li, J. Gaydos, and A. Neumann, Correlation of line tension and solid-liquid interfacial tension from the measurement of drop size dependence of contact angles, J. Colloid Interface Sci. **169**, 256 (1995).
[25] Y. Takata, H. Matsubara, Y. Kikuchi, N. Ikeda, T. Matsuda, T. Takiue, and M. Aratono, Line tension and wetting behavior of an air/hexadecane/aqueous surfactant system, Langmuir **21**, 8594 (2005).
[26] M. Kanduč, L. Eixeres, S. Liese, and R. R. Netz, Generalized line tension of water nanodroplets, Phys. Rev. E **98**, 032804 (2018).
[27] J. Włoch, A. P. Terzyk, and P. Kowalczyk, New forcefield for water nanodroplet on a graphene surface, Chem. Phys. Lett. **674**, 98 (2017).
[28] J. Zhang, P. Wang, M. K. Borg, J. M. Reese, and D. Wen, A critical assessment of the line tension determined by the modified Young's equation, Phys. Fluids **30**, 082003 (2018).
[29] G. Scocchi, D. Sergi, C. D'Angelo, and A. Ortona, Wetting and contact-line effects for spherical and cylindrical droplets on graphene layers: A comparative molecular-dynamics investigation, Phys. Rev. E **84**, 061602 (2011).
[30] M. Khalkhali, N. Kazemi, H. Zhang, and Q. Liu, Wetting at the nanoscale: A molecular dynamics study, J. Chem. Phys. **146**, 114704 (2017).
[31] B. M. Law, S. P. McBride, J. Y. Wang, H. S. Wi, G. Paneru, S. Betelu, B. Ushijima, Y. Takata, B. Flanders, and F. Bresme, Line tension and its influence on droplets and particles at surfaces, Prog. Surf. Sci. **92**, 1 (2017).
[32] A. Amirfazli and A. Neumann, Status of the three-phase line tension: A review, Adv. Colloid Interface Sci. **110**, 121 (2004).
[33] B. Pethica, The contact angle equilibrium, J. Colloid Interface Sci. **62**, 567 (1977).
[34] L. Boruvka and A. Neumann, Generalization of the classical theory of capillarity, J. Chem. Phys. **66**, 5464 (1977).
[35] R. C. Tolman, The effect of droplet size on surface tension, J. Chem. Phys. **17**, 333 (1949).
[36] P.-G. de Gennes, F. Brochard-Wyart, and D. Quéré, *Capillarity and Wetting Phenomena: Drops, Bubbles, Pearls, Waves* (Springer Science & Business Media, New York, 2013).
[37] R. David and A. W. Neumann, Empirical equation to account for the length dependence of line tension, Langmuir **23**, 11999 (2007).
[38] See Supplemental Material at http://link.aps.org/supplemental/10.1103/PhysRevLett.130.064003 for derivations of the main equations, details of the numerical implementation, and validation efforts.
[39] B. Shapiro, H. Moon, R. L. Garrell, and C.-J. Kim, Equilibrium behavior of sessile drops under surface tension, applied external fields, and material variations, J. Appl. Phys. **93**, 5794 (2003).
[40] M. Iwamatsu, A generalized Young's equation to bridge a gap between the experimentally measured and the theoretically calculated line tensions, J. Adhes. Sci. Technol. **32**, 2305 (2018).
[41] D. Kim, N. M. Pugno, M. J. Buehler, and S. Ryu, Solving the controversy on the wetting transparency of graphene, Sci. Rep. **5**, 15526 (2015).
[42] F. Taherian, V. Marcon, N. F. van der Vegt, and F. Leroy, What is the contact angle of water on graphene?, Langmuir **29**, 1457 (2013).
[43] T. Werder, J. H. Walther, R. Jaffe, T. Halicioglu, and P. Koumoutsakos, On the water- carbon interaction for use in molecular dynamics simulations of graphite and carbon nanotubes, J. Phys. Chem. B **107**, 1345 (2003).
[44] W. A. Steele, The physical interaction of gases with crystalline solids: I. Gas-solid energies and properties of isolated adsorbed atoms, Surf. Sci. **36**, 317 (1973).
[45] D. W. Siderius and L. D. Gelb, Extension of the steele 10-4-3 potential for adsorption calculations in cylindrical, spherical, and other pore geometries, J. Chem. Phys. **135**, 084703 (2011).
[46] B. Ramos-Alvarado, S. Kumar, and G. Peterson, Wettability of graphitic-carbon and silicon surfaces: Md modeling and theoretical analysis, J. Chem. Phys. **143**, 044703 (2015).
[47] B. Ramos-Alvarado, Water wettability of graphene and graphite, optimization of solid-liquid interaction force fields, and insights from mean-field modeling, J. Chem. Phys. **151**, 114701 (2019).
[48] J. H. Weijs, A. Marchand, B. Andreotti, D. Lohse, and J. H. Snoeijer, Origin of line tension for a Lennard-Jones nanodroplet, Phys. Fluids **23**, 022001 (2011).
[49] M. Shao, J. Wang, and X. Zhou, Anisotropy of local stress tensor leads to line tension, Sci. Rep. **5**, 9491 (2015).
[50] R. Bey, B. Coasne, and C. Picard, Probing the concept of line tension down to the nanoscale, J. Chem. Phys. **152**, 094707 (2020).
[51] M. E. M. Azouzi, C. Ramboz, J.-F. Lenain, and F. Caupin, A coherent picture of water at extreme negative pressure, Nat. Phys. **9**, 38 (2013).
[52] B. J. Block, S. K. Das, M. Oettel, P. Virnau, and K. Binder, Curvature dependence of surface free energy of liquid drops and bubbles: A simulation study, J. Chem. Phys. **133**, 154702 (2010).
[53] Ø. Wilhelmsen, D. Bedeaux, and D. Reguera, Tolman length and rigidity constants of the Lennard-Jones fluid, J. Chem. Phys. **142**, 064706 (2015).
[54] Y. A. Lei, T. Bykov, S. Yoo, and X. C. Zeng, The Tolman length: Is it positive or negative?, J. Am. Chem. Soc. **127**, 15346 (2005).
[55] S. Wang, X. Wang, B. Zhao, L. Wang, J. Qiu, L. Zhou, Y. Dong, B. Li, J. Lü, and Y. Wang, Size-dependent stiffness of nanodroplets: A quantitative analysis of the interaction between an afm probe and nanodroplets, Langmuir **32**, 11230 (2016).

[56] P. Attard and S. J. Miklavcic, Effective spring constant of bubbles and droplets, Langmuir **17**, 8217 (2001).
[57] P. Attard, Direct measurement of the surface tension of nanobubbles, arXiv:1505.02217.
[58] E. E. Meyer, K. J. Rosenberg, and J. Israelachvili, Recent progress in understanding hydrophobic interactions, Proc. Natl. Acad. Sci. U.S.A. **103**, 15739 (2006).
[59] J. N. Israelachvili and G. E. Adams, Measurement of forces between two mica surfaces in aqueous electrolyte solutions in the range 0–100 nm, J. Chem. Soc., Faraday Trans. 1 **74**, 975 (1978).
[60] J. N. Israelachvili, *Intermolecular and Surface Forces* (Academic, New York, 2011).
[61] N. Eom, D. F. Parsons, and V. S. Craig, Roughness in surface force measurements: Extension of DLVO theory to describe the forces between Hafnia surfaces, J. Phys. Chem. B **121**, 6442 (2017).
[62] R. Seemann, S. Herminghaus, and K. Jacobs, Dewetting Patterns and Molecular Forces: A Reconciliation, Phys. Rev. Lett. **86**, 5534 (2001).
[63] H.-J. Butt, K. Graf, and M. Kappl, *Physics and Chemistry of Interfaces* (John Wiley & Sons, New York, 2013).
[64] J. L. Parker, P. M. Claesson, and P. Attard, Bubbles, cavities, and the long-ranged attraction between hydrophobic surfaces., J. Phys. Chem. **98**, 8468 (1994).